Dark mode-in-the-box for enhanced second-harmonic generation in corrugated waveguides

Anne-Laure Fehrembach, François Renaud, Evgeny Popov, Herve Tortel, Antoine Monmayrant, Olivier Gauthier-Lafaye, Stephane Calvez

Dark mode-in-the box for enhanced second-harmonic generation in corrugated waveguides

ANNE-LAURE FEHREMBACH[1], FRANÇOIS RENAUD[1,2], EVGENY POPOV[1,3], HERVE TORTEL[1], ANTOINE MONMAYRANT[2], OLIVIER GAUTHIER-LAFAYE[2], STEPHANE CALVEZ[2]

[1] *Aix Marseille Univ, CNRS, Centrale Marseille, Institut Fresnel, F-13013 Marseille, France*
[2] *LAAS-CNRS, Université de Toulouse, CNRS, 7 avenue du colonel Roche, F-31400 Toulouse, France*
[3] *Institut Universitaire de France, Paris, France*
**Corresponding author: e.popov@fresnel.fr*

Abstract: A numerical study of second-harmonic generation (SHG) in cavity resonator integrated grating filters (CRIGFs) shows extraordinary strong conversion rates in planar corrugated waveguides based on Lithium Niobate layers, not exceeding 625 µm in length. The key idea is to couple to the dark mode of the structure at the pump frequency that has a Q-factor much stronger than the bright mode commonly used. This is achieved by shifting the grating coupler between the enclosing Bragg mirrors, resulting in an asymmetric structure. Three asymmetric structures are proposed: without any matching, with impedance matching and with indirect phase matching through an additional pair of gratings. They offer respectively increasing conversion rates of $\eta=4.31\times10^{-3}$, 0.149 & 2.38 W^{-1}, which compared to a symmetric CRIGF ($\eta=7.12\times10^{-6}$ W^{-1}) offer respectively more than 2, 4 and 5 orders of magnitude improvement of the conversion rate.

1. Introduction

Nonlinear optical frequency conversion and, in particular, second-harmonic generation (SHG), plays an important role in laser systems, infrared imaging, and signal detection. Guided-wave optics presents natural advantages in SHG device design mainly resulting from the ability to confine light in small volumes and thereby to reach the high-power densities needed to achieve efficient nonlinear conversion. Planar technology uses grating couplers (GCs) not only for light in/out-coupling into waveguides, but also to provide double resonances by inducing phase matching between the waveguide modes at the pump and the signal frequencies. Since the early 1990s, different configurations have been proposed to efficiently confine light in 2D and 3D planar or strip waveguide cavities and photonic crystals [1-13]. Different designs for phase matching use additional gratings, sometimes generated by electrical poling [14].

Weak conversion rates allow for the so-called undepleted pump approximation that neglects the inverse up-conversion in which the signal is sufficiently strong to influence the pump field. In this approximation, the generated SHG power is proportional to the square of the pump power or equivalently to the 4^{th} power of the waveguide-mode amplitude at the pump frequency, pointing out the importance of efficient light coupling.

The waveguide mode excitation in GCs results in stronger electromagnetic fields when the quality factor Q of the device is the largest possible [15]. However, due to the intrinsic property of such devices, the larger the Q-factor, the tighter the angular tolerances, both being linked by the grating equation [16]. Therefore, the required geometrical dimensions are large, restricting the possibility of strong incident light focusing. A way to avoid this restriction is to couple light

through the waveguide edges; recently quite strong conversion factors have been reported in the literature [14]. However, this design is incompatible with planar-coupling technology.

Another method to enlarge the angular tolerance is to put a small size GC in between two Bragg Gratings (BGs) forming a Fabry-Perot (FP) resonator. This geometry, called cavity resonator integrated grating filter (CRIGF) [17] introduces almost angularly flat mode dispersion curves and gives rise to efficient mode coupling using focused beams with waists down to several micrometers, preserving Q-factors up to several thousand [18]. Theoretical and experimental studies show the possibility of efficient SHG comparable to other technologies [19].

In almost all the previous studies, the structures are designed to make use of the so-called bright waveguide modes, for which electric field extrema are aligned with the center of the grooves and bumps. However, it is well-known that dark modes [20] have Q-factors largely exceeding those of bright modes, simply because the former are weakly excited thus the imaginary part of their propagation constant is small. Their excitation is possible, for example, under oblique incidence, but at the expense of an increased excitation volume.

In this paper, we show that shifting the central GC within the FP resonator, thereby introducing an asymmetry, facilitates the excitation of a dark mode with high Q-factor while preserving the incidence close to normal, and maintaining strong focusing of the incident light. We demonstrate a mode-amplitude enhancement inducing more than 5 orders of magnitude improvement in conversion efficiency η compared to the more conventional symmetric CRIGF design. In the next two sections, we present the optogeometrical parameters of the CRIGF design followed by a short analysis of the bright and dark modes for infinite central GCs. Section 4 describes a first asymmetric CRIGF enhancing conversion efficiency by more than 2 orders of magnitude compared to the symmetrical CRIGF. In sec. 5 we propose a second and improved asymmetric CRIGF where a simple trick allows a reduction of the effective index mismatch between different sections of the CRIGF, resulting in a 4-order-of-magnitude improvement in η (compared to the symmetrical CRIGF). Section 7 presents a third and last asymmetric CRIGF with an extra pair of gratings ensuring indirect phase match between the fundamental waveguide modes at the pump and signal frequencies. With such phase matching, η improves by more than 5 orders of magnitude (compared to the symmetrical CRIGF).

2. CRIGF structure

The vertical stack for all the CRIGF structures under study here is described on figure 1, together with the refractive indices of each layer at both the fundamental (ω) and signal (2ω) frequencies. Note that the refractive index dispersion around each of the frequencies will be neglected. This theoretical stack was designed respecting technological fabrication constraints of previously reported samples [19].

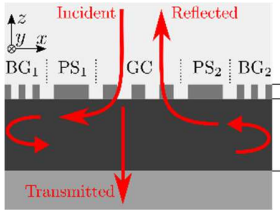

			ω	2ω
$1/2\ \infty$	air	n_A	1.0000	1.0000
37 nm	Si_3N_4	n_G	1.9963	2.0259
300 nm	$LiNbO_3$	n_L	2.1362	2.1793
$1/2\ \infty$	SiO_2	n_S	1.4440	1.4538

Figure 1: (left) overall planar geometry of the CRIGF consisting of 5 sections (inwards: 2 Bragg gratings BG1 & BG2, 2 phase sections PS1 & PS2 and 1 central grating coupler GC); (right) description of the vertical stack.

This stack consists of a 300-nm-thick Lithium Niobate layer on a silica substrate [21], acting as a single-mode waveguide. We consider semi-infinite air superstrate and silica substrate. On top of the waveguide a 37-nm-thick Si_3N_4 layer is deposited and then dry-etched to form the grating layer. The reference CRIGF structure consists of three gratings and two phase sections (PSs). A central grating coupler (GC) is sided by two PSs and two Bragg Gratings (BGs) closing a Fabry-Perot cavity around the GC, thus confining the waveguide mode at the pump frequency under the GC. The current technological process imposes the same groove depth for all three gratings. The groove depth of 37 nm is chosen as a compromise to simultaneously provide relatively weak mode coupling by the GC and sufficiently strong mode reflection by the BGs at the pump frequency to limit the losses in the BG parts of the waveguide and maintain the ability to create an overall high Q-factor device.

The four CRIGFs studied here all use the same vertical stack and overall longitudinal structure consisting of 5 sections: two Bragg gratings BG_1 & BG_2, two phase sections PS_1 & PS_2 and one central grating coupler GC, as described in figure 1. They only differ by the particular content and geometry of the grating layer inside the PS_1, PS_2 and GC sections, as described in figure 2.

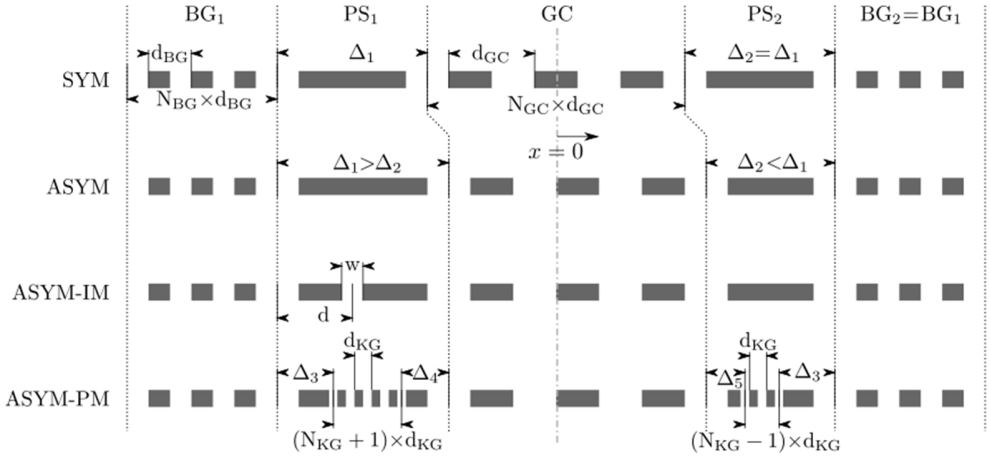

Figure 2: Description of the grating layer for the 4 CRIGF geometry under study: (SYM) symmetric CRIGF serving as a reference with identical PS and BG on each side; (ASYM) asymmetric CRIGF where the GC is laterally shifted by increasing the left PS while keeping the cavity size constant; (ASYM-IM) asymmetric CRIGF with an extra groove in the left PS to ensure impedance matching for the mode; (ASYM-PM) asymmetric CRIGF with an extra pair of gratings in both PS to ensure indirect phase-matching of fundamental and signal in the structure (KG). This last structure is significantly larger than the 3 others (not to scale).

The *x* axis corresponds to the longitudinal direction in the cavity and its origin is defined at the center of the symmetric CRIGF (SYM) and the distances are calculated between the groove centers at the end of each sections. In all four structures, the gratings (coupler GC, reflectors BG and phase-matching KG) all have a filling factor (or duty cycle) of 50%. Moreover, the number of periods and periodicity of the GC and of both BGs are constant: N_{GC}=21, d_{GC}=884 nm, N_{BG}=400, $d_{BG}=d_{GC}/2$=442 nm. How these values are chosen is explained in section 4.

Our reference structure is the symmetric CRIGF (SYM) where both PS have the same length $\Delta_1=\Delta_2$=986 nm. The first asymmetric structure (ASYM) has a longer left PS and a shorter right PS ($\Delta_1>\Delta_2$) in order to shift the central GC by around $d_{GC}/4$, while keeping the cavity length constant. A first improvement over this asymmetric design is to reduce the impedance mismatch occurring at the long left PS_1 interfaces: in the impedance-matched asymmetric

CRIGF (ASYM-IM), an extra notch is etched in PS_1, while keeping the right-side PS_2 unchanged. The last structure ASYM-PM uses significantly longer PS_1 & PS_2 that contains an additional grating KG to ensure indirect phase-matching between the fundamental and signal guided modes, together. Note that while the 3 first structures have similar length (around 375 µm), the last one is longer (around 625 µm).

3. Dark and bright modes of the central grating coupler

As in our previous [19] studies, we first consider the symmetrical design (SYM) where the GC is positioned symmetrically between the BGs, under normal incidence. Provided that the length of the resonator is appropriately tuned by choosing the correct ($\Delta_1=\Delta_2$) phase shift distance between the GC and the BGs, light injection in the device excites the hybrid symmetrical mode of the GC and FP resonator system.

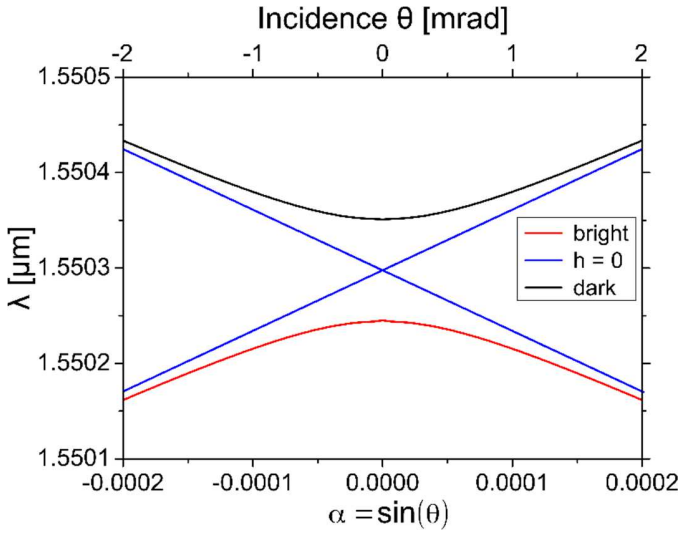

Figure 3: Dispersion curves of the waveguide mode of an infinitely long grating, corresponding to the GC of CRIGF. Red curve, the bright branch, black curve, the dark branch, blue lines, without the grating (grating height h=0). Wavelength λ=1.55 µm, TE polarization.

Figure 3 presents the map of the mode dispersion curves for both the symmetric and the antisymmetric mode of an infinitely long GC. Throughout the paper, we present the mode amplitude and electric field values as calculated at the waveguide lower cladding interface.

The spectral width of the symmetrical mode (lower wavelength branch) and its mode amplitude are insignificantly affected by the change of incident direction, characterized with angle θ. Only its spectral position varies, following the dispersion curves shown in Fig. 3. As mentioned, the antisymmetric mode cannot be excited under normal incidence, therefore the imaginary part of its propagation constant is null, its Q-factor is infinite, and the mode amplitude is zero. This can be observed on the spectral dependence of the reflectivity, where only the anomaly due to the symmetric mode appears for θ=0. The reflectivity spectrum shows a broad peak corresponding to the low Q factor of the bright mode. When the symmetry is broken by choosing an inclined incidence, the excitation of the antisymmetric mode creates another Fano-type anomaly in the reflectivity (Fig. 4(a)) which appears as a dip in the broad reflectivity peak of the symmetric mode. Increasing the angle of incidence decreases the asymmetric-mode Q-factor, increases the anomaly width and decreases the amplitude of the guided mode (Fig. 4(b)). For example, for an incident angle of 0.1 mrad, the Q-factor is equal to 70 000 and it decreases

to 3 400 at 0.4 mrad incidence. This is to be compared with the approximately constant Q-factor of 300 of the symmetric mode.

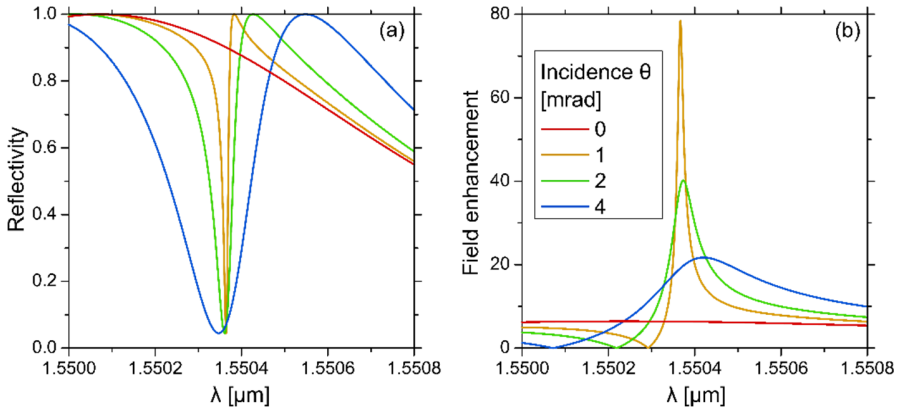

Figure 4: (a) The reflectivity spectrum of the infinite GC for different angles of incidence; (b) The corresponding electric field enhancement (with respect to the incident field) at the lower guide interface for a plane incident wave.

These considerations may seem trivial and well-known, but we prefer to summarize them with respect to the properties of the more complex systems discussed further on. It is important to highlight that for a grating, with a symmetry with respect to the vertical plane as is above, the Fano-type anomaly is characterized, at least theoretically, by a 100 % reflectivity at maximum [22, 23]. Another property is that the spectral position of the anomaly strongly depends on the angle of incidence leading to very tight angular tolerances.

4. CRIGFs in symmetric and antisymmetric configurations

As already demonstrated [24], when a finite portion of a grating as considered above is placed in a resonator, its dispersion curves are flattened permitting large Q-factors under excitation by a focused incident beam. The effect is used to design narrow-band single-layer spectral filters, external laser mirrors, and can lead to enhanced SHG without phase matching. To compare the efficiency of each configuration of CRIGFs, we use the definition of the conversion power factor η as the ratio between the intensity power $P_{2\omega}$ radiated by the system at the signal frequency and the square of the incident power at the pump frequency P_ω: $\eta=P_{2\omega}/(P_\omega)^2$.

Typically, a conversion factor of the order of 10^{-5} was observed in CRIGFs [19], i.e. more than 10^3 times larger than what is achievable with bulk configurations with similar volumes.

Throughout the paper, and as in ref. [19], SHG calculations are made with a home-made numerical code based on the Fourier Modal Method, under the undepleted pump approximation [25, 26]. The finite size of the CRIGF component along x is considered by applying the so called "super-cell" approach [27], and both the structure and the incident Gaussian beam are invariant along the perpendicular direction to the plane of Fig. 1 (2D beam). Considering 3D beams would be too costly in computation time. We have validated our Fourier Modal Method code by comparison with another of our home-made numerical code based on the Finite Element Method. We aim at calculating quantitative SHG powers (not in arbitrary units) and be able to compare them with the real case of a 3D Gaussian beam. To do so, we calculate the power of our 2D-beams (pump and harmonic) as the flux of the Poynting vector over a surface perpendicular to z, covering the length of the CRIGF along x, and with a width along y such that this power is equal to that of a true 3D beam with the same waist. As explain in the Appendix, the length along y must be $1.25w_0$. All the results presented here are obtained for excitation under normal incidence by a TE-polarized focused beam with a waist of 9 μm and

1W power, for the sake of simplicity. The results for a more realistic case of smaller incident power, for example 1mW, can be simply deduced by multiplying the field amplitude at ω by $10^{-3/2}$ and the SHG power by 10^{-6}, as calculations at 2ω are linear with respect to the pump field at the square.

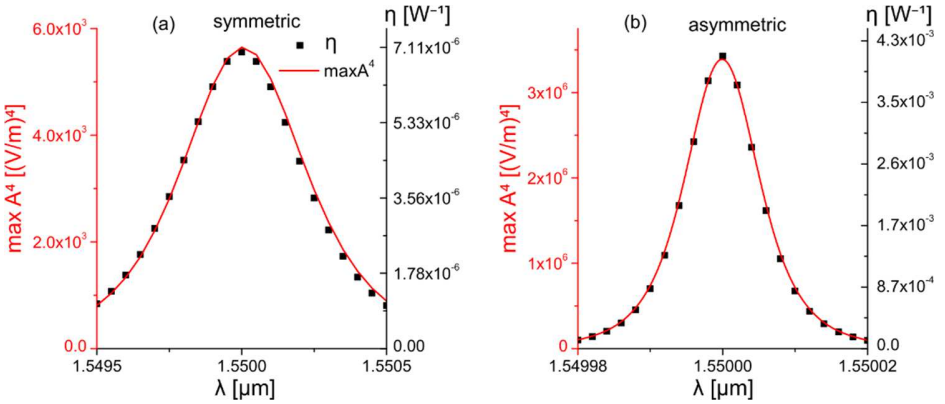

Figure 5: Spectral dependence of the fourth power of the pump mode amplitude at ω (red line) and the SHG conversion factor (black squares) of the (a) symmetric (SYM) and b) asymmetric (ASYM) structures.

The first symmetric structure SYM described in Fig. 2 with $\Delta_1=\Delta_2$, supports a single waveguide mode at 1.55 μm with effective propagation index $n_{eff}=1.7534$. In normal incidence this mode requires a grating coupler with period $d_{GC}=884$ nm. Filling ratio of 0.5 is chosen to provide the most efficient coupling. The BGs have half of the period d_{GC}, a filling factor of 0.5, too, and work in the middle of their band gap. Typically, $N_{BG}=400$ periods are largely sufficient to ensure 0.999 reflectivity of the waveguide mode. This SYM structure is designed with symmetric PS of $\Delta_1=\Delta_2=986$ nm that brings the FP resonance at 1.55 μm wavelength. Similar geometry had already been studied theoretically and its properties confirmed experimentally [19], thus it can serve as a reference. Spectral dependence of the SHG conversion factor is shown in Fig. 5(a), together with the dependence of the forth power of the waveguide mode amplitude at the pump frequency. As seen, the emitted second harmonic power is strictly proportional to the pump mode amplitude 4^{th} power since, under the undepleted pump approximation, the non-linear polarization P^{NL} is proportional to the square of the mode field at ω, and the SHG power, to the square of the generated field at 2ω.

The values of the Q-factor, peak spectral reflectivity at the fundamental wavelength $R_{max}(\lambda)$, mode amplitude A inside the CRIGF for the fundamental wavelength and SHG conversion efficiency η are presented in Table 1 together with all the other investigated structures.

Table 1. Optical properties of the different CRIGFs.

Structure	$R_{max}(\lambda)$ [%]	Q-factor	Mode Amplitude A [$V.m^{-1}$]	η [W^{-1}]	η/η(SYM)
SYM	88	1 700	8.64	$7.12\ 10^{-6}$	1.00
ASYM	49	57 000	43.02	$4.31\ 10^{-3}$	$6.05\ 10^{+2}$
ASYM-IM	77	290 000	101.50	0.149	$2.09\ 10^{+4}$
ASYM-PM	70	1 900 000	268.00	2.38	$3.34\ 10^{+5}$

As expected, a symmetric structure used in symmetric incidence (symmetric Gaussian beam in normal incidence) can only excite a symmetric mode whose mode amplitude and Q-factor approach those of its infinite-long central grating coupler. The main difference is that the CRIGF permits focused beams with much larger power density, thus significantly larger SHG.

If the central GC segment is displaced with respect to the BG box at a distance approximately equal to $d_{GC}/4$=221 nm, it is possible to excite a symmetric FP mode with the same symmetric incidence but this mode becomes antisymmetric with respect to the GC. That is the basic principle guiding the design of our first asymmetric CRIGF ASYM. In practice, because the incident beam is not a plane wave, a numerical optimization of the optogeometrical parameters is necessary. The best results (maximum mode amplitude and SHG) are obtained for a displacement equal to 204 nm instead of the expected 221 nm, resulting in Δ_1=1190 nm and Δ_2=782 nm. This difference can be explained by the fact that in reality the field is neither completely symmetric nor antisymmetric.

As can be seen in Table 1, comparing the SYM and ASYM structures, the use of the antisymmetric mode of the GC leads to a 5-fold increase in the mode amplitude, leading to a 625 (5^4) increase in the SHG power in the undepleted pump approximation. The Q-factors of the spectral width of the two configurations are of the same orders of magnitude as those of the symmetric and antisymmetric modes of the infinite gratings as discussed in Sec. 3.
Kintaka et al. [28] already reported a theoretical 6-fold increase of the Q-factor by displacing the GC position. In our case the increase is greater than 33 times.

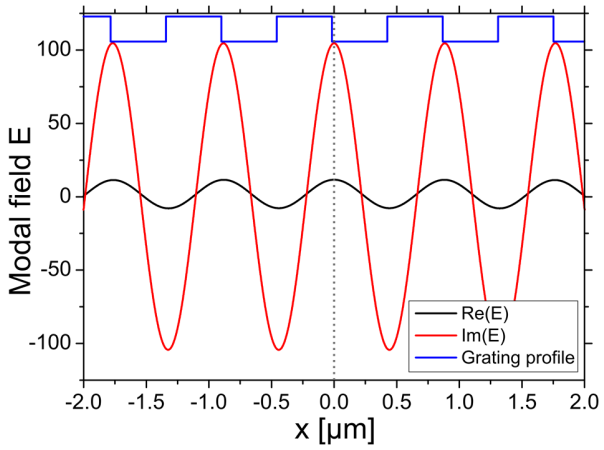

Figure 6: Spatial electromagnetic field distribution for the asymmetric structure ASYM in close vicinity of the system center. The blue line represents the GC profile, shifted with respect to x = 0.

The spatial distribution of the modal field in the ASYM structure, shown in Fig. 6, confirms that (1) it is almost symmetric with respect to the FP box, and antisymmetric for the GC, and (2) it is close to being purely harmonic, representing a standing wave formed by the waveguide mode at ω with n_{eff}=1.754. The field at 2ω is created by the square of the field at ω and thus has the same symmetry. Note that at 2ω, the GC acts as a diffractive grating sustaining the 0^{th} and $\pm1^{st}$ orders extraction and the BG sections serve as close-to-surface-normal output coupling gratings. As a result, the device behaves as a singly-resonant nonlinear converter with high SHG extraction efficiency. Most of SHG outcoupling is made in the GC and BG parts (around 40% in the cladding and 60% in the substrate, only less than 1% is guided out through the ends on the waveguide region). We plot in Fig. 7 the normalized modulus of the electric field at x=0

with respect to *z*, at the pump and harmonic frequencies, showing the confinement of the mode at the pump frequency inside the Lithium Niobate layer.

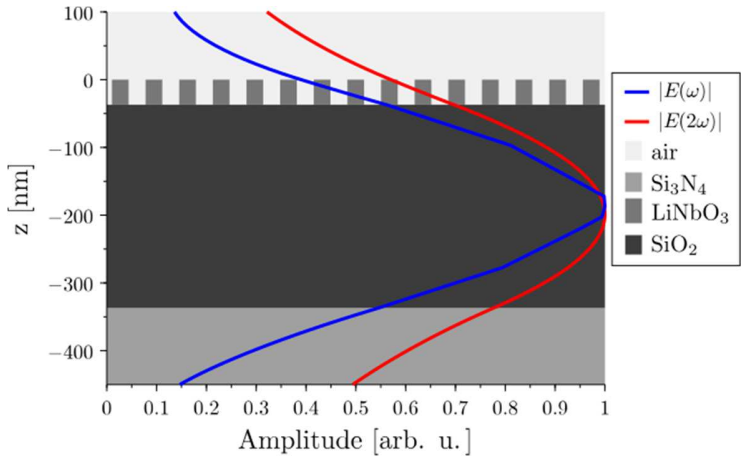

Figure 7: Normalized modulus of the electric field at x=0 with respect to *z*, at the pump and harmonic frequencies.

The structure of the electric field in CRIGF is relatively well understood in the linear regime, but it is much more complex in SHG nonlinear regime. In our case, the guiding structure supports a single mode. As already discussed, inside the GC and BG parts it has a normalized propagating constant close to n_{eff}=1.754. The period of GC is chosen to excite this mode close to normal incidence. The Bragg mirrors reflect back this mode into the central part without diffracting it into the substrate and cladding, neglecting the transition losses and the scattering losses due to the finite size of the system. The backscattering force can be expressed as an extinction coefficient equal to 4.46 10^{-2} μm^{-1}.

5. Further improvements of asymmetric CRIGFs: ASYM-IM

We observed in the previous section that using an already large-amplitude pump field can greatly enhance the signal. However, theoretically high Q-factor can be reduced significantly by any type of losses. Already existing indication points out the unexpected behavior of the ASYM structure: the maximum value of reflection at the pump frequency in the spectral dependence is equal to 49 % for ASYM structure, much lower than the value of 88 % for SYM structure, the latter being typical for usual CRIGFs, indicating the presence of losses in the structure. We assume no absorption losses, the leakage outside the box in the lateral direction is minimized by the efficient Bragg mirrors, and the waist of the incident beam that is optimized to the size of the central grating coupler. Reducing the structure losses to increase even more the amplitude of the pump field implies thus reducing the transition losses between the different parts on the CRIGF structure.

We have already chosen the GC and BGs periods to match well the modes in these sections. Indeed, n_{eff} of the waveguide mode at ω in the GC is equal to 1.75402 + i 4.78 10^{-4}, and in the BG to 1.75340 + i 1.1 10^{-2}. However, there is a flat region between them, namely the phase shifts PS_1 and PS_2. If short enough, PS does not perturb the mode propagation due to tunneling. However, in the ASYM CRIGF (see Fig. 2), the first phase shift PS_1 is optically longer than 1.5 wavelengths. If the shift is considered infinitely long, n_{eff} of the mode inside such region is equal to 1.7718, considerably different from the grating regions. Although not affecting the total energy balance, this can introduce scattering losses for the waveguide modes. In order to study their role, we introduced additional small-width groove inside PS_1, so that it can reduce the average optical index and thus match the n_{eff} of the adjacent regions.

The structure ASYM-IM in Fig. 2 and Table 1 is practically identical to ASYM, but with an additional groove in PS_1 of width w=170 nm, situated at a distance d=423 nm of the left side of PS_1, both values of w and d resulting from numerical optimization. For this new structure, the reflectivity spectral maximum at ω increases to 77 %. Moreover, this modification leads to a further increase of the mode field amplitude and SHG power. It translates into a predicted conversion efficiency of $\eta=0.149\ W^{-1}$ and corresponds to an improvement of more than 4 orders of magnitude with respect to our reference structure (see Table 1). This ASYM-IM structure thus approaches the best conversion efficiency described in the literature, while preserving the planar geometry, normal illumination, small dimensions (less than 375 µm total length for 50 µm transverse width [27]), and less than 1 mm total thickness, including the substrate.

From there, additional improvements can be done, but at the expense of increasing the device dimensions. There are two major and complementary approaches to do so. The first technique exploits the fact that the Q-factor depends linearly on the FP resonator length, as long as the quality of the mirrors and the coherence of the modes under consideration are maintained along the entire structure. It must be stressed that the aforementioned results are obtained without phase match between the modes at ω and 2ω. The second approach is based on improving the modal overlap between the pump and signal fields. It turns out to be difficult to directly match their effective indices due to the material and geometric dispersion. However, additional grating [29] can be used to introduce indirect mode matching through the mutual coupling of the signal and pump waves. Of course, this also leads to an increase in the cavity length.

6. Indirect phase matching: ASYM-PM

We introduce two additional gratings (named KG), within the two PS sections PS_1 and PS_2, as described in Fig. 2. The K-gratings have a period of d_{KG}=206 nm, suitable to couple the fundamental modes at ω and 2ω through the first diffracted order. Thus, an enhancement of the fundamental mode at 2ω is achieved. The small pitch does not permit propagating diffraction orders in the cladding nor in the substrate. A 50 % duty cycle ensures the match of the effective indexes of the modes in the different regions and around N_{KG}=600 periods are used. Contrary to the previous two geometries, the asymmetrical position of the GC with respect to the BG can be achieved simply by choosing a different number of grooves for the two additional gratings, namely $N_{KG}+1=601$ in PS_1 and $N_{KG}+1=599$ in PS_2. Thus, the total length of the system is increased by approximately 248 µm, reaching 625 µm. In addition to these gratings, the phase sections PS_1 and PS_2 also contains unstructured regions for optimization (see Fig. 2 for definitions). Numerical optimization leads to lengths Δ_3=489 nm and Δ_4=436 nm in PS_1 and Δ_3 =489 nm and Δ_5= 419 nm in PS_2. This optimization results in a conversion efficiency $\eta=2.38\ W^{-1}$ (Table 1, last line), more than 5 orders of magnitude improvement as compared to our reference structure. The field spatial distribution remains the same as in Sec. 4, see Fig. 6, because, first, in the undepleted pump approximation the transfer of energy from the pump to the signal frequency does not affect the pump field distribution, and second, the additional KG does not diffract in the surrounding media. The mode amplitude is therefore constant in the GC and KG, and decreases exponentially in the BG.

7. Achievements and difficulties

The SHG conversion factor of $\eta=2.38\ W^{-1}$ for a 625-µm-long system is several magnitudes larger than achieved in planar grating systems, and comparable to the best results obtained in other systems [14] that are several times longer. The reason for this high conversion is three-fold: (1) volume reduction inside the waveguide in vertical direction and Bragg resonator (in x), and (2) efficient excitation with focused incident beam of the dark mode, combined with (3) an indirect phase matching at pump and signal frequencies. This leads to extremely high Q-factors of the pump modal field. However, the tolerances for the fabrication of such resonant

structure will be quite challenging, requiring extremely low technologically-induced-losses processing, and nanometer scale precision for the most stringent designs.

The other difficulty for longer systems (ASYM-PM structure with phase-matching additional gratings) is the divergence of the waveguide modes due to the 3-dimensional geometry, as a focused incident beam creates waveguide modes that diverge when propagating in the guide, and when reflected back by the Bragg mirrors. The longer the system in *x*, the larger the conversion. In order to limit the effect of this divergence that limits pump energy concentration, it is necessary to introduce a lateral confinement, either using a ribbon guide [14] or an optical index modification (for example by proton exchange in the $LiNbO_3$ guiding layer) or using concave Bragg mirrors [30].

The last structures in Table 1 presents SHG conversion factor >1 W^{-1}, which means that a pump power of 1 W is supposed to generate >1 W signal. It is well known that this nonphysical deviation of the energy balance is due to the undepleted pump approximation – the energy transfer into signal frequency does not affect the pump field energy in this approximation. For such strong SHG it is necessary to consider a coupled set of differential equations simultaneously at ω and 2ω. Nevertheless, the results presented in Table 1 are useful for cases with lower pump power, where the approximation is still valid – for example, 1 mW pump power is supposed to generate "only" 2.38 μW of second-harmonic power, i.e. the reduction of the pump power will be less than 0.24 %, sufficiently small to be neglected.

8. Conclusion

A numerical optimization study of second-harmonic generation (SHG) in cavity resonator integrated grating filters (CRIGFs) has been carried out. For sub-625-μm-long structures, by combining the excitation of a dark-mode of the structure at the pump frequency, that has a Q-factor much stronger than the bright mode commonly used, with an impedance matching scheme and with an indirect phase matching through an additional pair of gratings, increased conversion rates by respectively more than 2, 4 and 5 order of magnitude improvement are predicted.

The chosen materials, Silicon Nitride and Lithium Niobate, the geometry and the dimensions are compatible with actual technological fabrication constraints with e-beam lithography and dry etching. We believe that this study confirms the potential of CRIGF for non-linear effect enhancement, in particular SHG conversion. It also paves the way for an even stronger enhancement, using the phase matching properties that a more elaborated layer stack can bring.

9. Appendix: Estimation of the conversion factor for a 3D incident Gaussian beam

For the 2D Gaussian beam with beam radius at waist w_0, we write the electric field as $E = E_0 \exp\left[-\left(\frac{x}{w_0}\right)^2\right]$ in the plane of the waist. The 1D-flux of the Poynting vector through an infinite line along *x* is then written

$$P^{2D} = \frac{1}{2\mu_0 c} w_0^2 E_0^2 k_0^2 I_0,$$

where $k_0 = \frac{2\pi}{\lambda}$ and λ the wavelength, $\mu_0 c$ the vacuum impedance, and $I_0 = \int_0^1 \mathrm{d}u \exp\left(\frac{-(uk_0 w_0)^2}{2}\right)\sqrt{1-u^2}$.

For the 3D Gaussian beam, we write the electric field as $\mathrm{E} = \mathrm{E}_0 \exp\left[-\left(\frac{r}{w_0}\right)^2\right]$ in the plane of the waist, in polar coordinates with radius *r*. The flux of the Poynting vector though an infinite surface in the plane of the waist then is written

$$P^{3D} = \frac{\pi}{4\mu_0 c} w_0^4 E_0^2 k_0^3 I_1,$$

where $I_1 = \int_0^1 \mathrm{d}u\, u \exp\left(\frac{-(uk_0 w_0)^2}{2}\right)\sqrt{1-u^2}$.

We thus have $\frac{P^{3D}}{P^{2D}} = \frac{I_1}{2I_0}\pi w_0^2 k_0$, a conversion factor that is nearly constant and equal to (1.25±0.3%) w_0 for w_0>2λ.

Hence, the flux of the Poynting vector of the 2D Gaussian beam through a surface infinite along *x*, and with length $1.25w_0$ along the direction of invariance *y*, will be equal to that of the 3D Gaussian beam through an infinite surface.

Data availability. Data underlying the results presented in this paper are not publicly available at this time but may be obtained from the authors upon reasonable request.

Funding. RESON - 19-ASTR-0019-01

Acknowledgments. F. Renaud acknowledges PhD Grant from DGA/AID.

Disclosures. The authors declare no conflicts of interest.

References

1. G. Blau, E. Popov, F. Kajzar, A. Raimond, J. Roux, and J. Coutaz, "Grating-assisted phase-matched second-harmonic generation from a polymer waveguide," Opt. Lett. **20**, 1101-1103 (1995).
2. A. Cowan and J. Young, "Mode matching for second-harmonic generation in photonic crystal waveguides," Phys. Rev. B **65**, 085106 (2002).
3. M. Siltanen, S. Leivo, P. Voima, M. Kauranen, P. Karvinen, P. Vahimaa, and M. Kuittinen, "Strong enhancement of second-harmonic generation in all-dielectric resonant waveguide grating," Appl. Phys. Lett. **91**, 111109 (2007).
4. G. Poberaj, H. Hu, W. Sohler, and P. Günter, "Lithium niobate on insulator (LNOI) for micro-photonic devices," Laser Photon. Rev. **6**, 488-503 (2012).
5. C. Wang, K. Zhaoyi, L. Myoung-Hwan, X. Xiong, X.-F. Ren, G.-C. Guo, N. Yu, and M. Loncar, "Metasurface-assisted phase-matching-free second harmonic generation in lithium niobate waveguides," Nat. Commun. **8**, 2098 (2017).
6. C. Wang, X. Xiong, N. Andrade, V. Venkataraman, X.-F. Ren, G.-C. Guo, and M. Loncar, "Second harmonic generation in nano-structured thin-film lithium niobate waveguides," Opt. Express **25**, 6963-6973 (2017).
7. M. Borghi, C. Castellan, S. Signorini, A. Trenti, and L. Pavesi, "Nonlinear silicon photonic," J. Opt. **19**, 093002 (2017).
8. A. Boes, B. Corcoran, L. Chang, J. Bowers, and A. Mitchell, "Status and potential of Lithium Niobate on Insulator (LNOI) for photonic integrated circuits," Laser Photonics Reviews **12**, 1700256 (2018).
9. J. Bravo-Abad, S. Fan, S. Johnson, J. Joannopoulos, and M. Soljacic, "Modeling Nonlinear Optical Phenomena in Nanophotonics," J. Lightwave Technol. **25**, 2539-2546 (2007).
10. N. Segal, S. Keren-Zur, N. Hendler, and T. Ellenbogen, "Controlling light with metamaterial-based nonlinear photonic crystals," Nat. Photonics **9**, 180-184 (2015).
11. A. D. Logan, M. Gould, E. R. Shmidgall, K. Hestroffer, Z. Lin, W. Jin, A. Majumdar, F. Hatami, A. W. Rodriguez, and K.-M. C. Fu, "400%/W second harmonic conversion efficiency in 14 μm-diameter gallium phosphide-on-oxide resonators," Opt. Express **26**, 33687-33699 (2018).
12. A. Krasnok, M. Tymchenko, and A. Alù, "Nonlinear metasurfaces: a paradigm shift in nonlinear optics," Mater. Today 21(1), 8-21 (2018).
13. R. Mohsen, G. Leo, I. Brener, A. V. Zayats, S. A. Maier, C. De Angelis, H. E. A. Tan, V. F. Gili, F. Karouta, R. Oulton, K. Vora, M. Lysevych, I. Staude, L. Xu, A. E. Miroshnichenko, C. Jagadish, and D. N. Neshev. "Nonlinear frequency conversion in optical nanoantennas and metasurfaces: materials evolution and fabrication," Opto-Electronic Adv. **1**, 180021 (2018).
14. C. Wang, C. Langrock, A. Marandi, M. Jankowski, M. Zhang, B. Desiatov, M. M. Fejer, and M. Loncar, "Ultrahigh-efficiency wavelength conversion in nanophotonic periodically poled lithium niobate waveguides," Optica **5**, 1438–1441 (2018).

15. Y. H. Ko, N. Gupta, and R. Magnusson, "Resonant filters with concurrently tuned central wavelengths and sidebands," Opt. Lett. **45**, 6046-6049 (2020).
16. E. Popov and B. Bozhkov: "Corrugated waveguides as resonance optical filters – advantages and limitations," J. Opt. Soc. Am. A **18**, 1758-1764 (2001).
17. K. Kintaka, T. Majima, J. Inoue, K. Hatanaka, J. Nishii, and S. Ura, "Cavity-resonator-integrated guided-mode resonance filter for aperture miniaturization," Optics express **20**, 1444–1449 (2012).
18. X. Buet, E. Daran, D. Belharet, F. Lozes-Dupuy, A. Monmayrant, and O. Gauthier-Lafaye, "High angular tolerance and reflectivity with narrow bandwidth cavity-resonator-integrated guided-mode resonance filter," Opt. Express **20**, 9322-9327 (2012)
19. F. Renaud, A. Monmayrant, S. Calvez, O. Gauthier-Lafaye, A.-L. Fehrembach, and E. Popov, "Second-harmonic-generation enhancement in cavity resonator integrated grating filters," Opt. Lett **44**, 5198-5201 (2019).
20. T. Wu, M. Gurioli, and P. Lalanne, "Nanoscale lightr confinement: the Q's and V's," ACS Photonic **8**, 1522-1538 (2021)
21. Q. Yifan and L. Yang, "Integrated lithium niobate photonics," Nanophotonics, **9**, 1287-1320 (2020).
22. E. Popov, L. Mashev and D. Maystre, "Theoretical Study of the Anomalies of Coated Dielectric Gratings," Opt. Acta **33**, 607 (1986).
23. S. S. Wang, R. Magnusson, J. S. Bagby, and M. G. Moharam, "Guided-mode resonances in planar dielectric-layer diffraction gratings," J. Opt. Soc. Am. A **7**, 1470-1474 (1990).
24. N. Rassem, A.-L. Fehrembach, and E. Popov, "Waveguide mode in the box with an extraordinary flat dispersion curve," J. Opt. Soc. Am. A **32**, 420-430 (2015).
25. W. Nakagawa, T. Rong-Chung, and Y. Fainman, "Analysis of enhanced second-harmonic cgeneration in periodic nanostructures using modified rigorous coupled-wave analysis in the undepleted-pump approximation," J. Opt. Soc. Am. A **19**, 1919-1928 (2002).
26. B. Bai and J. Turunen:."Fourier modal method for the analysis of second-harmonic generation in two-dimensionally periodic structures containing anisotropic materials," J. Opt. Soc. Am. B **24**, 1105-1112 (2007).
27. P.C. Chaumet, G. Demésy, O. Gauthier-Lafaye, A. Sentenac , E. Popov, and A.-L. Fehrembach, "Electromagnetic modeling of large subwavelength-patterned highly resonant structures," Opt. Lett. **41**, 2358-2361 (2016).
28. K. Kintaka, K. Asai, K. Yamada, J. Inoue and S. Ura, "Grating-Position-Shifted Cavity-Resonator- Integrated Guided-Mode Resonance Filter," IEEE Photonics Technology Lett., **29**, 201-204, (2017)
29. R. Reinisch, M. Nevière, and E. Popov, "Phase-matched guided wave optical bistability in c(2) optical resonator," Opt. Lett. **20**, 2472-2474 (1995).
30. Y. Mao, J. Zhu, K. Li, B. Du, and X. Hou, "Perfect matching of concave diffraction grating with continuously circular Bragg mirrors on SOI platform," J. Opt. Soc. Am. A **36**, 641-646 (2019)